This article has been accepted for publication in a future issue of this journal, but has not been fully edited. Content may change prior to final publication. Citation information: DOI 10.1109/LAWP.2015.2391293, IEEE Antennas and Wireless Propagation Letters

Nitrogen Dioxide Wireless Sensor based on Carbon Nanotubes and UWB RFID Technology

Angel Ramos, Pierrick Clément, Antonio Lazaro, *Member, IEEE,* Eduard Llobet, *Senior Member, IEEE*, David Girbau, *Senior Member, IEEE*

***Abstract*—This paper presents a semi-passive wireless nitrogen dioxide gas sensor based on a time-coded ultra-wideband tag. The gas is sensed by means of oxygen-plasma-treated multiwall carbon nanotubes. The reader consists of a commercial ultra-wideband radar. The signal backscattered at the tag is modulated by a single-pole double-throw switch and contains information on the gas concentration. The tag is normally in sleep mode and includes a wake-up circuit. A self-calibration circuit is also included, enabling two additional measurements used for background subtraction and calibration to be obtained. The sensor is able to detect nitrogen dioxide concentrations from 10 ppm to 100 ppm, with a mean relative error of 0.34%.**

***Index Terms*—Ultra-wideband, RF Switch, carbon nanotubes, nitrogen dioxide gas sensor**

I. Introduction

WIRELESS sensing of hazardous gases is a subject that has been under research recently [1]. Some gases such as ammonia (NH_3), carbon dioxide (CO_2) and nitrogen dioxide (NO_2), are potentially hazardous for humans, as well as for livestock and agriculture. Carbon nanotubes (CNTs) may be an enabling technology for detecting these gases since they provide a large specific surface area to interact with their environment, their electrical conduction changes dramatically upon gas absorption, and response and recovery of CNT sensors operated at room temperature has been reported [2].

Several investigations have aimed to detect gases using CNT-based sensors integrated into passive or semi-passive RFID tags. For instance, a multiwall CNT-based CO_2, O_2 and NH_3 passive wireless sensor was presented in [3], based on an inductor-capacitor resonant circuit and providing measurements at a 15 cm reader-tag distance. Single-wall CNTs were used as an impedance loading on a conventional passive RFID 915 MHz tag in [4], detecting 6 ml of 10% of NH_3 at a reader-tag distance of 63.5 cm.

In cases [3-4], narrowband signals were used. However, recent works [5] have demonstrated that ultra-wideband (UWB) signals can also be used for RFID applications. This paper presents a semi-passive RFID NO_2 sensor based on a time-coded UWB backscatterer. The UWB backscatterer is loaded with an RFIC single-pole double-throw (SPDT) switch. The switch's actuation voltage is modulated by an oxygen-plasma-treated multiwall CNT-based sensor, which enables NO_2 to be detected at room temperature. The tag also integrates a wake-up and self-calibration circuit, which saves battery life and enables measurements in time-variant scenes.

The paper is organized as follows. Section II presents the operation principle. Section III experimentally characterizes the RFIC switch and the tag performance. Section IV presents the reader and the CNT-based sensor. Section V presents the results measured and the proposed calibration method. Finally, Section VI shows the conclusions.

II. Operation Principle

Fig. 1 shows a diagram of the sensor tag, based on a UWB backscatterer topology, and the signals sent from (TX) and backscattered to the reader (RX). The reader transmits a pulse *p(t)*. When this pulse hits the tag, a portion of it is backscattered (addressed as structural mode) and another portion propagates inside the tag (addressed as tag mode). The tag response is therefore composed of the sum of these two terms. The structural mode depends on the shape and size of the tag and the material of which it is made. The tag mode depends on the radiation characteristics of the antenna and the load connected to it [5]. Here the tag is based on a UWB antenna connected to a delay line (L_1), which is in turn connected to the input J_1 of a commercial RFIC SPDT switch (Skyworks AS186-302LF). The two outputs of the switch, J_2 and J_3, are connected to two open-ended delay lines, L_2 and L_3 respectively. It is important to note that length $L_2 \neq L_3$. Hence the tag modes associated with positions J_2 and J_3 of the switch have different structural-to-tag mode delays, and therefore each can be distinguished from the other.

III. Time-Domain Modulation using an RF Switch

This section studies the modulation of the tag mode amplitude using the AS186-302LF switch. According to the manufacturer, to connect J_1 with J_2, the V_1 input must be in a high voltage state (3 V) whereas the V_2 is in a low voltage state (0 V). Similarly, to connect J_1 with J_3, V_1 = 0 V and V_2 = 3 V. Here, intermediate values of V_1 within this range are considered to intentionally change its insertion loss and modulate the amplitude of the tag mode associated with the J_2 output (which depends on V_1). A tag made of a UWB antenna connected to a coaxial line of length L_1, with a round-trip

Paper submitted July 22, 2014. This work was supported by Spanish Government Project TEC2011-28357-C02-01, Agaur Grant 2013FI_B1 00060 and an ICREA Academia Award.

The authors are with the Department of Electronics, Electrics and Automatic Control Engineering, Rovira i Virgili University, Tarragona, Av. Països Catalans 26, 43007 Tarragona, Spain. (e-mail: david.girbau@urv.cat).

This article has been accepted for publication in a future issue of this journal, but has not been fully edited. Content may change prior to final publication. Citation information: DOI 10.1109/LAWP.2015.2391293, IEEE Antennas and Wireless Propagation Letters

delay of 2.3 ns is designed. The other end of L_1 is connected to input J_1 of the switch. Outputs J_2 and J_3 of the switch are left to an open circuit without any line ($L_2 = 0$) and connected to another coaxial line of length $L_3 = L_1$ respectively. Tag modes 1 and 2 are therefore time-separated 2.3 ns. V_1 here is driven by a controllable power supply. The tag is measured by the commercial UWB radar Time Domain PulsON P400.

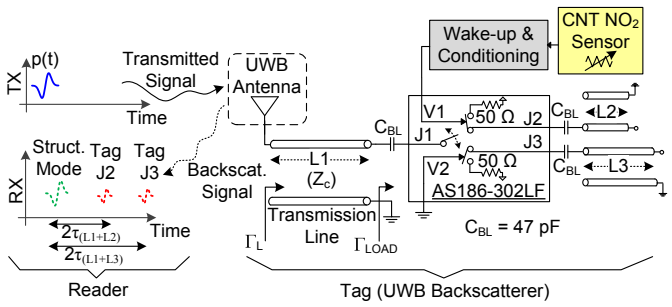

Fig. 1. Diagram of the UWB sensor and the TX and RX signals at the reader.

Fig. 2.a shows the time-domain response of the tag as a function of V_1 measured at a 50 cm tag-reader distance. The continuous wavelet transform (CWT) processing technique [5] is applied to all the measurements to reduce noise. Measurements are normalized with respect to the absolute maximum, which is the structural mode. It can be seen that while the structural modes remain invariant, the tag modes vary depending on V_1. There is an exploitable zone in the 1 – 1.4 V region (marked with a green shadow) which can be used to modulate the tag mode. Figs. 2.b-c show the amplitudes of the normalized tag modes (1 and 2) for 8 consecutive measurements with the radar. Measurements using switches with different production dates and at different temperatures have been done. A repeatable behaviour is observed. Tag mode 1 is exploited to sense and tag mode 2 is used for identification by changing length L_3. The switch measured maximum current consumption is 0.25 µA. Therefore, it is a perfect candidate as an RF transducer in battery-powered wireless sensors. In this work, only one of the states is exploited (V_2 is grounded). However, since there are two possible modes, two sensors could be measured, taking into account the voltage requirements at V_1 and V_2.

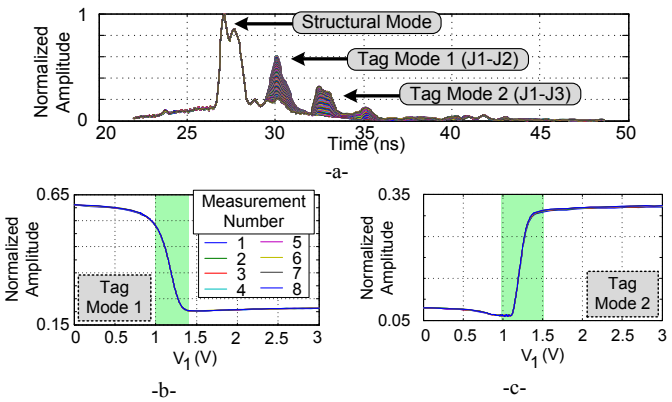

Fig. 2. (a) Time-domain response of the tag as a function of V_1, measured by the UWB radar. (b) Amplitudes of tag mode 1 and (c) of tag mode 2.

IV. System Design

A. Reader

Fig. 3 shows a diagram of the proposed reader-tag system. The reader consists of the UWB radar (PulsON P400) and a wake-up transmitter. The wake-up transmitter sends a modulated 2.45 GHz tone to activate the tag, which is normally in sleep mode. The radar then obtains the UWB backscattered reply.

The 2.45 GHz wake-up tone is generated by a Mini-Circuits ROS 2793-119+ oscillator, connected to a power amplifier (Mini-Circuits Gali-24+) and a monopole antenna. The modulation of the wake-up tone is done by switching the oscillator on or off with an on-off keying (OOK) scheme. It is carried out from the control PC via USB, using a Microchip PIC16F1827 microcontroller. The inset in Fig. 3 shows the modulation scheme in detail. Two states (S_1 and S_2) are generated by switching the oscillator with duty cycles of 33% and 66% respectively. In the S_1 state, the tag sets the RFIC switch actuation voltage V_1 to depend on the CNT. In the S_2 state, the tag sets V_1 to a fixed 3 V value for calibration.

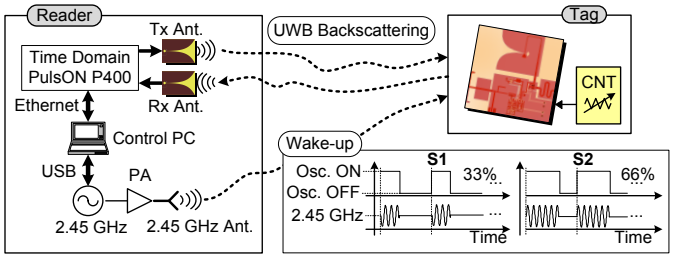

Fig. 3. Diagram of the proposed reader-tag system.

B. Tag design

Fig. 4 shows a photograph of the tag. It is fabricated on a Rogers RO4003C substrate and measures 120 mm x 120 mm. It consists of a UWB Vivaldi antenna connected to the RFIC switch. $L_2 = 0$ mm and the L_3 round-trip delay is 850 ps. For convenience, the CNT is placed on a separate board and wire-connected to the sensor tag, marked CNT in Fig. 4 (left). A reference connector (marked Ref in Fig. 4) is used to measure voltage V_1 for sensor verification and first-time calibration. The tag is powered by a 3 V lithium battery. Fig. 5 shows the circuit scheme of the wake-up, conditioning and calibrating circuit. It consists of a 2.45 GHz dipole antenna connected to a detector based on a Schottky diode rectifier (Avago HSMS-2852). It is connected to a rail-to-rail operational amplifier (Texas Instruments TLV2401) that acts as a comparator. The threshold value for this comparator is generated by an RC filter used as mean estimator (R = 82 kΩ, C = 1 µF). A second RC filter (R = 820 kΩ, C = 1 µF) is connected to the output of the comparator to calculate the mean voltage (V_{Mean}) of the OOK signal. This mean voltage depends on the duty cycle (33% or 66%) and is independent of the reader-tag distance because of the first comparator, which acts as a buffer. The output of the second RC filter (V_{Mean}) is connected to the non-inverting inputs of two additional comparators, with thresholds of 0.55 V and 1.33 V (obtained from two resistive divisors at V_{CC}). The outputs of the two comparators define the S_1 and S_2 states. Output S_2 is used as a control voltage for

This article has been accepted for publication in a future issue of this journal, but has not been fully edited. Content may change prior to final publication. Citation information: DOI 10.1109/LAWP.2015.2391293, IEEE Antennas and Wireless Propagation Letters

a MAX4523 DC switch, whose output is the actuation voltage V_1 of the RF switch. When 0.55 V < V_{Mean} < 1.33 V, S_1 = 3 V and S_2 = 0 V. This is called state S_1, which corresponds to the NO_2 measurement state. Here a fourth operational amplifier is activated, turning on the signal conditioner circuit of the CNT. Its output V_{CNT} depends on the NO_2 concentration. Since output S_2 = 0 V, $V_1 = V_{CNT}$. However, when V_{Mean} > 1.33 V, S_1 = S_2 = 3 V. This is called state S_2, which corresponds to the calibration state. In this case $V_1 = S_2 = 3$ V.

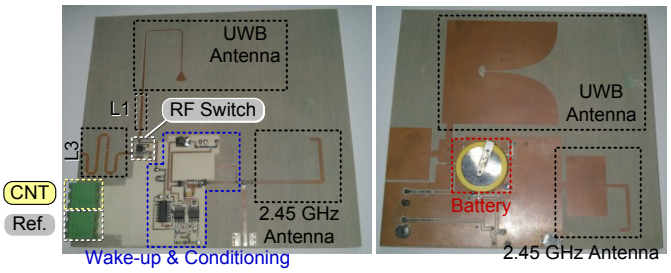

Fig. 4. Photograph of the fabricated tag, front (left) and back (right).

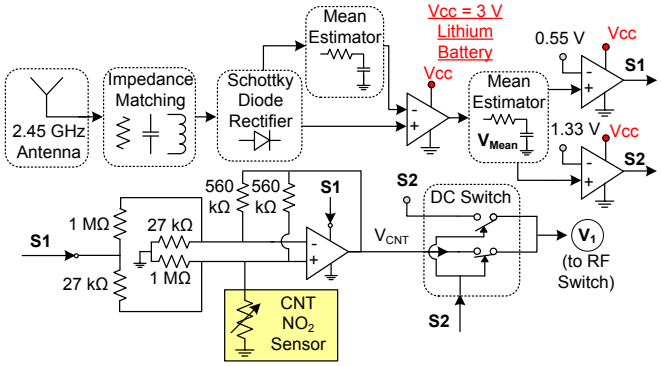

Fig. 5. Circuit diagram of the wake-up, conditioning and calibrating circuit.

C. CNT gas sensor

The multiwall carbon nanotubes (MWCNT) used in the experiment were obtained from Nanocyl, S.A. (Belgium). They are synthesized by chemical vapour deposition and have a purity of over 95%. They measure up to 50 microns in length and their outer and inner diameters range from 3 to 15 nm and 3 to 7 nm respectively. A uniform functionalization with oxygen is applied to the carbon nanotubes provided so as to improve their dispersion and surface reactivity. This functionalization has been found to enhance sensitivity towards NO_2 [2,6]. Different functionalizations of carbon nanotubes (e.g. surface decoration with metal or metal oxide nanoparticles) can be envisaged to tune the sensitivity toward volatile organic compounds [7]. In the second processing step, the functionalized carbon nanotubes are dispersed in an organic vehicle (dimethylformamide), ultrasonically stirred for 20 min at room temperature and then air-brushed onto the sensor substrate while the resistance of the resulting film during deposition is controlled.

Fig. 6.a shows the manufactured CNT sensor. It consists of an interdigital copper structure which series-connects input and output. The MWCNT is deposited over this interdigital structure. Fig. 6.b shows the gas chamber that has been designed to house the sensor, while Fig. 6.c shows a detail of the chamber cap with the flow tubes.

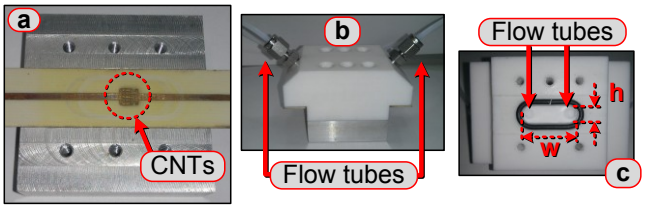

Fig. 6. Photographs of the substrate with the CNT sensor (a), of the closed gas chamber with the access flow tubes (b) and of the conduit with the open chamber (c). Size of the chamber: w = 23.5 mm x h = 7.35 mm.

Fig. 7 shows the evolution of sensor resistance as a function of the NO_2 concentration. It consists of successive response-recovery cycles at increasing concentrations (10, 30, 50, 70 and 100 ppm) of NO_2. Each response-recovery cycle consists of 10 minutes of exposure to diluted NO_2 followed by 100 minutes recovery in dry air. A moderate baseline drift can be observed. However, the baseline is recovered in full when the duration of the cleaning cycle is increased to 140 minutes or more. The experiments were performed at room temperature.

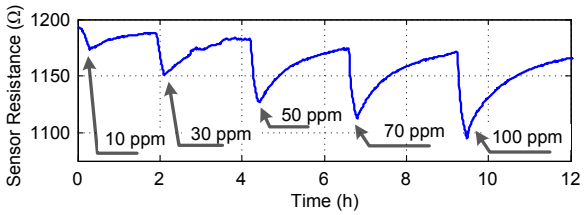

Fig. 7. Response and recovery cycles of a CNT sensor operated at room temperature. The evolution of sensor resistance for several concentrations of NO_2 is shown.

V. Results

The measurements here reported are carried out at a tag-reader distance of 1 m, because of gas laboratory limitations. However, larger read-ranges can be achieved with semi-passive UWB RFID [5]. Fig. 8 shows the unprocessed UWB signal as a function of V_1 for voltages from 0 V to 3 V. A large coupling contribution from the reader transmitter to the receiver antenna and clutter due to reflections from nearby objects in the scene can be observed, masking the tag response. In order to reduce these contributions, the time-domain signal measured with V_1 = 0 V is used as the background and subtracted from all measurements. Thus the coupling and clutter contributions are subtracted because they do not depend on the tag mode. This enables a background subtraction to be performed before each measurement, and hence a time-variant background is not a problem for the sensor. The structural mode is also heavily reduced. This is where the importance of the second tag mode can be seen. The sensor must now be identified from the time difference between the tag 1 and tag 2 modes, since the structural mode is no longer useful for this purpose. Fig. 9 shows the time-domain signal after the background subtraction and after the continuous wavelet transform has also been applied. All signals are normalized with respect to the case of V_1 = 3 V. An inset in Fig. 9 shows the amplitudes of the tag 1 modes as a function of V_1 (normalized to V_1 = 3 V). An interpolation is calculated for the RF switch operation region using the piecewise cubic Hermite interpolating polynomial. This curve is used as the sensor's calibration curve.

This article has been accepted for publication in a future issue of this journal, but has not been fully edited. Content may change prior to final publication. Citation information: DOI 10.1109/LAWP.2015.2391293, IEEE Antennas and Wireless Propagation Letters

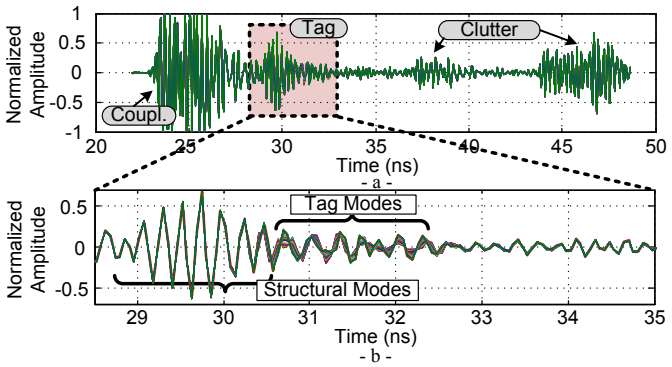

Fig. 8. Raw UWB signal as a function of V_1 (a) and zoomed tag response (b).

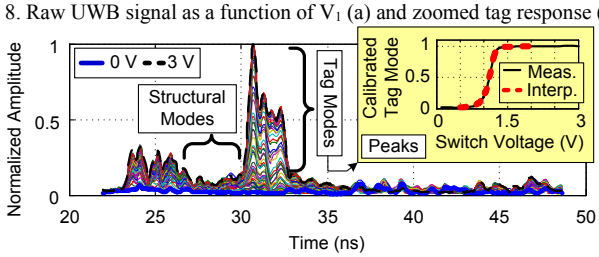

Fig. 9. Time-domain signals after background subtraction and after applying the CWT, normalized to the case of 3 V.

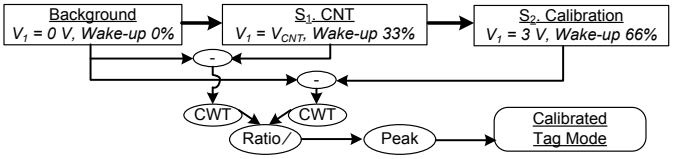

Fig. 10. Flow diagram for one calibrated measurement.

The sensor measurement requires three steps, as shown in Fig. 10. First the background is measured without sending any wake-up signal (V_1 = 0 V). Then tag state S_1 is measured with the wake-up duty cycle at 33% ($V_1 = V_{CNT}$). Finally state S_2 is measured with the wake-up duty cycle at 66% ($V_1 = S_2$ = 3 V). The background is subtracted from the measurements at states S_1 and S_2. Then the CWT is applied to the S_1 and S_2 states. Finally S_1 is calibrated with respect to S_2, and the maximum peak of the tag mode is obtained. This process enables measurements at any angle or distance (within the read range) between tag and reader to be obtained. No measurement of the scene without the tag is necessary for background subtraction.

Three cycles consisting of 100 ppm of NO_2 for 10 min and air for 100 min are injected into the gas chamber. The estimated voltage at the RF switch (V_1) is obtained from the calibrated tag mode and shown in Fig. 11. For reference purposes, a wired DC multimeter is connected in parallel to monitorize V_1. A repeatable pattern can be observed, and the wireless measurement is very close to the multimeter reference. In order to detect several concentrations of NO_2, Fig. 12 shows the relative resistance change from the calibrated tag mode. The resistances are obtained from calculations using the conditioning circuit in Fig. 5. Then, the relative resistance is considered from the initial value at t = 0 h. Relative changes of 3.9%, 9.2%, 14%, 16.6%, and 19.9% are obtained for 10, 30, 50, 70 and 100 ppm respectively. The maximum relative error is 1.5% and the mean relative error is 0.34%.

As regards power consumption, the RF switch consumes a maximum measured current of 0.25 µA, each operational amplifier consumes 0.88 µA, the DC switch 1 µA and the conditioning circuit 100 µA. In total, the tag consumes 105.5 µA in states 1 and 2 (NO_2 and calibration measurements respectively) and 4.3 µA in the sleep mode and background measurement.

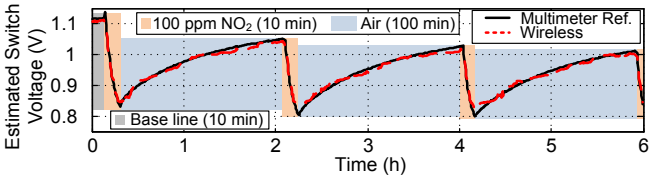

Fig. 11. Estimated switch voltage V_1 as a function of time for three measurement cycles of 100 ppm NO_2 compared to measured voltage V_1.

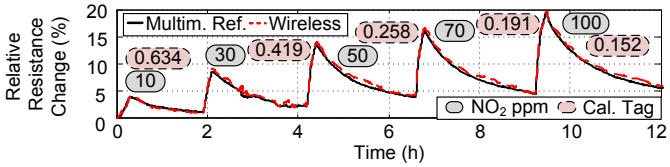

Fig. 12. Relative resistance change as a function of NO_2 concentration, and corresponding measured calibrated tag mode.

VI. Conclusion

This paper has presented a wireless NO_2 sensor based on oxygen-plasma-treated multiwall carbon nanotubes integrated into a time-coded ultra-wideband tag. The sensor is based on modulating the amplitude of the tag mode by means of an RF switch. A wake-up circuit enables the tag to be powered up only when it has to perform a measurement. A self-calibration circuit and a method based on the measurement of two fixed states in addition to the gas concentration measurement enables the tag to operate independently of the tag-reader distance or angle and without the need to perform a measurement of the empty scene for background subtraction. The sensor was measured for several NO_2 concentrations between 10 ppm and 100 ppm and a reader-sensor distance of 1 meter, with relative changes of between 3.9% and 19.9% respectively being obtained, with 0.34% mean relative error. The sensor is suitable for alarms and air quality monitoring.

References

[1] T. T. Thai, L. Yang, G. R. DeJean, and M. M. Tentzeris, "Nanotechnology Enables Wireless Gas Sensing," *IEEE Microwave Magazine*, pp. 84-95, 2011.

[2] Z. Zanolli, R. Leghrib, A. Felten, J-J. Pireaux, E. Llobet, J-C. Charlier, "Gas Sensing with Au-Decorated Carbon Nanotubes", *ACS Nano*, 5, Vol. 6, pp. 4529-4599, 2011.

[3] K. G. Ong, K. Zeng, and C. A. Grimes, "A Wireless, Passive Carbon Nanotube-Based Gas Sensor," *IEEE Sensors Journal*, Vol. 2, No. 2, pp. 82-88 2002.

[4] C. Occhiuzzi, A. Rida, G. Marrocco, and M. M. Tentzeris, "RFID Passive Gas Sensor Integrating Carbon Nanotubes," *IEEE Trans. On Microwave Theory and Tech.*, Vol. 59, No. 10, pp. 2674-2684. 2011.

[5] A. Ramos, A. Lazaro, and D. Girbau, "Semi-Passive Time-Domain UWB RFID System," *IEEE Transactions on Microwave Theory and Techniques*, Vol. 61, No. 4, pp. 1700-1708, 2013.

[6] R. Ionescu et. al., "Oxygen functionalisation of MWNT and their use as gas sensitive thick-film layers," *Sensors and Actuators B*, 113, pp. 36-46, 2006.

[7] P. Clément et. al., "Iron oxide and oxygen plasma functionalized multi-walled carbon nanotubes for the discrimination of volatile organic compounds," *Carbon*, Vol. 78, pp. 510-520, Nov. 2014.